

Diurnal ocean surface warming drives convective turbulence and clouds in the atmosphere

Simon P. de Szoeke

Oregon State University, Corvallis, OR, USA

simon.deszoeke@oregonstate.edu

Tobias Marke

CIRES, University of Colorado Boulder

NOAA Chemical Sciences Laboratory, Boulder, CO, USA

tobias.marke@noaa.gov

W. Alan Brewer

NOAA Chemical Sciences Laboratory, Boulder, CO, USA

alan.brewer@noaa.gov

Key Points

- A vast area of the ocean surface warms in the afternoon under calm winds, enhancing surface buoyancy flux to the atmosphere.
- Diurnally enhanced buoyancy flux from the ocean generates a diurnal convective turbulent mixed layer in the atmosphere.
- Enhanced afternoon marine atmospheric turbulence forms clouds by mixing moisture to its condensation level.

Abstract

Sunlight warms sea surface temperature (SST) under calm winds, increasing atmospheric surface buoyancy flux, turbulence, and mixed layer depth in the afternoon. The diurnal range of SST exceeded 1 °C for 24% of days in the central tropical Indian Ocean during the Dynamics of the Madden Julian Oscillation experiment in October-December 2011. Doppler lidar shows enhancement of the strength and height of convective turbulence in the atmospheric mixed layer over warm SST in the afternoon. The turbulent kinetic energy dissipation of the marine atmospheric mixed layer scales with surface buoyancy flux like previous measurements of convective mixed layers. The time of enhanced mixed layer dissipation is out of phase with the buoyancy flux generated by nocturnal net radiative cooling of the atmosphere. Diurnal atmospheric convective turbulence over the ocean mixes moisture from the ocean to the lifting condensation level and forms afternoon clouds.

Plain language summary

Howard's (1803) original description of cumulus clouds includes convection (overturning by heating from below) in the heat of the afternoon. When wind is weak, sunlight warms vast and variable areas of the ocean (some 5% of the tropical oceans and 2% of Earth's surface) by more than 1 °C in the afternoon. Convection and turbulence form over the warmed ocean like over land. We show the afternoon strengthening and deepening of the turbulence. The afternoon

convection raises water vapor from the ocean surface, moistens the atmosphere, and forms clouds.

1. Introduction

Diurnal warming of the ocean surface is expected to generate turbulence, but measurements of the diurnal vertical profile of turbulence have never before been documented. The afternoon warming of the ocean is much weaker than that of land because the ocean mixes and stores heating over a depth of meters to tens of meters. Diurnal warm layers (DWLs) of sea surface temperature (SST) result from strong solar absorption and weak winds (Price et al. 1986, Fairall et al. 1996, reviewed in Kawai and Wada 2007). Clear skies result in more solar absorption. Weak winds result in weak turbulent fluxes and ocean mixing.

Many remote sensing- and model-based analyses show a significant fraction of days and locations have DWLs with diurnal SST range (dSST) greater than 1° C, with extremes exceeding 5° C in satellite analyses (Gentemann et al. 2003, Clayson and Bogdanoff 2013). One year of buoy observations in the tropical Atlantic Ocean show dSST exceeds 1°C for 8% of days, with slightly weaker dSST in collocated satellite observations (Clayson and Weitlich 2007). Diurnal SST modeled from 6-hourly ERA-40 (40-yr European Centre for Medium-Range Weather Forecasts Re-Analysis) is weaker than dSST observed by collocated drifters (Bellenger and Duvel 2009). Buoy observations from 5 sites show dSST exceeds 1°C for 5% of days (Fig. 1; Prytherch

et al. 2013). If dSST reaches 1.0 °C for 5% of days and locations in the tropical oceans, these DWLs represent roughly 2% of Earth's area.

Precipitating atmospheric convective clouds are strongest in the early morning over the tropical oceans (e.g. Gray and Jacobson 1977). Solar absorption in the atmosphere mitigates the destabilizing effect of thermal infrared cooling, and suppress convective clouds (Randall et al. 1991). A secondary maximum of precipitation has been observed in the early afternoon when there is diurnal warming of SST (Chen and Houze 1997, Bellenger et al. 2010). The lack of diurnal cycles in SST and boundary layer convection in general circulation models results in errors in the phase and amplitude of precipitating convection (Dai and Trenberth 2004, Tian et al. 2004).

In the tropics, dSST is strong under weak winds in areas of convergence and between storms. These conditions are most common in the eastern tropical Pacific intertropical convergence zone, in the convergence of Western Pacific summer monsoon westerlies and easterly trade winds, and during phases of suppressed precipitation of tropical intraseasonal variability such as the Madden Julian Oscillation (Clayson and Weitlich 2007, Gentemann and Akella 2018). Diurnal warm layers form under weak winds also in midlatitudes (Merchant et al. 2008), which we hypothesize affect air-sea interactions during the formation of some marine heatwaves (e.g. Holbrook et al. 2019, Amaya et al. 2020).

Diurnal warm layers observed in the Mirai Indian Ocean cruise for study of the MJO-convection Onset (MISMO) and Dynamics of the Madden Julian Oscillation (DYNAMO) experiments locally moistened and warmed the atmospheric boundary layer, destabilized the atmosphere for precipitating convection (Bellenger et al. 2010, Ruppert and Johnson 2015), and increased integrated atmospheric water vapor (Yasunaga et al. 2008). Unsaturated convective boundary layer circulations have been observed to be responsible for fluxes of heat and moisture to the free troposphere when clouds were suppressed (LeMone and Pennell 1976). Cloud resolving models show an afternoon increase in shallow convective clouds over the DWL (Ruppert and Johnson 2016).

Here we document the diurnal response of turbulence that connects warm SST in the afternoon to convective clouds. Turbulence over marine convective atmospheric mixed layers has been observed previously by aircraft (Lenschow 1970, Frisch and Ochs 1975, Fairall et al. 1980). Ground-based remote sensing allows us to profile the turbulence throughout the diurnal cycle. Diurnal intensification and deepening of the turbulent atmospheric mixed layer were observed by Doppler lidar over strong DWLs ($dSST > 1.5\text{ }^{\circ}\text{C}$) in the central Indian Ocean in late 2011 during the Dynamics of the Madden Julian Oscillation (DYNAMO) experiment (section 2). The mixed layer turbulence is shown to scale with the buoyancy flux like previously observed convective mixed layers, including diurnal mixing over land (section 3). Section 4 shows the connection of the turbulent mixed layer to the clouds and summarizes its effect for modeling atmospheric moist convective clouds over the ocean.

2. DYNAMO observations

a. The diurnal warm layer of SST in the Indian Ocean

The DYNAMO experiment in November-December 2011 sampled two cycles of intraseasonal atmospheric variability (Madden and Julian 1971), including suppressed and active phases of precipitating convective clouds. The DYNAMO median dSST was 0.58 °C, its maximum was 2.8 °C. The dSST was greater than 1 °C for 19 (25%) of the 77 DYNAMO days (Fig. 1), and greater than 1.5°C for 7 of the days. Diurnal warm layers also formed on the days before, between, and after two convective westerly wind bursts (Moum et al. 2014). The vertical structure of the ocean DWLs was observed from a ship (Moulin et al. 2017, Hughes et al. 2020), and by ocean gliders penetrating the surface (Matthews et al. 2014).

The 4 consecutive days Nov 13-16 had dSST > 1.8 °C (Fig. 1c, 2d). During this intraseasonal phase of suppressed precipitation, weak winds reduced mechanical generation of turbulence in the atmosphere and ocean and permitted the DWL to form in the ocean. SST warmed quickly during midday solar heating November 13-15 and cooled slowly at night (Figs. 1c, 2d). On November 16, SST increased only modestly during midday and then quickly increased 2°C after 16 local time (LT). Quick cooling events in the evenings of Nov 14 and 15 were related to pulses of wind exceeding 3 m s⁻¹.

b. Wind and buoyancy flux

Figure 1a, b, and c show the diurnal cycles of the wind, SST, and buoyancy flux for two month-long legs of the DYNAMO experiment (de Szoeke et al. 2015). Over the warm tropical Indian Ocean, the thermal expansion of air due to temperature and the lowering of molecular mass due to water vapor both contribute comparably to the buoyancy flux. Surface buoyancy flux $B(0)$ is positive and lognormally distributed, with $\text{median}[B(0)] = 3.7 \times 10^{-4}$ and $\text{mean}[B(0)] = 4.8 \times 10^{-4}$. The friction velocity $u_* = \sqrt{|\tau|/\rho} \approx 0.04U_{10\text{rel}}$ is about 0.1 m s^{-1} on weak wind days (Fig 1a).

Wind speed dominates daily to intraseasonal variability of the latent and sensible turbulent surface fluxes in DYNAMO (de Szoeke et al. 2015, de Szoeke et al. 2017). Average buoyancy flux is weak ($3 \times 10^{-4} \text{ m}^2 \text{ s}^{-3}$) for wind below 3 m s^{-1} (Fig. 1b). Mean wind from 6-14 LT is less than 2.6 m s^{-1} on each of the 7 days with $\text{dSST} > 1.5^\circ \text{C}$ (section 2a). The buoyancy flux is weaker on these weak wind days, yet the diurnal cycle of buoyancy flux is coherent, with maximum daylight buoyancy flux ($6 \times 10^{-4} \text{ m}^2 \text{ s}^{-3}$) 2.7 times greater than the predawn (0-6 h local) mean buoyancy flux.

c. Turbulence dissipation profiles

The diurnal enhancement of buoyancy flux generates turbulent convection in the sub-cloud boundary layer. The NOAA High-Resolution Doppler Lidar (HRDL; Grund et al. 2001, Wulfmeyer

and Janjic 2005) measured the radial velocity of the air toward or away from the scanner. Vertical velocities in the sub-cloud boundary layer in DYNAMO were sampled by pointing vertically for 10 minutes, alternated with constant-elevation azimuthal scans every 20 minutes.

We estimate the turbulent kinetic energy (TKE) dissipation rate ϵ (Kolmogorov 1941) in 10-minute windows above 250 m (Fig. 2a,c) from spectra of the inertial cascade of isotropic turbulence (Kaimal 1973; data at <https://esrl.noaa.gov/csl/groups/csl3/measurements/dynamo/calendar.php>). Below 330 m, we estimate dissipation from transverse structure functions of the radial velocity from azimuthal scans (Fig. 2c, Frehlich et al. 2006). Further details of the observations, lidar scan strategy, and dissipation calculations are summarized in supplement S1. Examples of the horizontal velocity structures at night and in the afternoon are shown in supplement S2.

Mixed layer depth D

Most profiles in Fig. 2a,c show turbulent mixed layers with $\epsilon \approx 10^{-4} \text{ m}^2 \text{ s}^{-3}$ below a quiescent layer with much weaker turbulence $\epsilon < 10^{-5} \text{ m}^2 \text{ s}^{-3}$. We define the mixed layer depth D as the lowest height at which ϵ is a factor of 3 smaller than the vertical mean of ϵ below that height. Mixed layer depths were diagnosed for 2008 profiles of dissipation in this manner (black dots Fig. 2a,c).

Convective mixed layers

173 Buoyancy flux dominates the generation of TKE in DYNAMO, as in most marine atmospheric
 174 mixed layers. The shear production of TKE is less than the buoyancy integral $w_*^3 = [B]D$, where
 175 $[B]$ is the mixed-layer mean buoyancy flux. The ratio of TKE generation by shear production
 176 u_*^3/κ to surface buoyancy flux $B(0)D$ in the mixed layer is equal the ratio $-L/D$ of the
 177 (negative) Monin-Obukhov length ($-L = u_*^3/\kappa B(0)$) to the mixed layer depth D . The daylight
 178 median $-L/D$ for all days is 0.016. The mixed layers during the days with the 7 strongest dSST
 179 have maximum $-L/D$ of 0.043 and median 0.0037.

180

181 We define those mixed layers as *convective* that meet the threshold $-D/L > 100$. One third
 182 (658) of the mixed layers diagnosed in DYNAMO are convective according to this condition. The
 183 ratio $-D/L$ is strongly dependent on the surface wind speed. Most of the convective mixed
 184 layers have surface wind speed less than 2 m s^{-1} . The ratio $-D/L$ decreases approximately as
 185 wind speed U^{-3} in the shear-driven regime, and as U^{-2} in the convective regime (not shown),
 186 consistent with wind stress proportional to U^2 and buoyancy flux proportional to U (as in bulk
 187 aerodynamic models, e.g. Liu et al. 1979, Fairall et al. 1996).

188

189 The mixed layers sampled November 13-16 (with dSST $> 1^\circ\text{C}$) were particularly convective, with
 190 $-D/L$ greater than 100 for 96% (239) of the 249 mixed layer depths D . The time-height series for
 191 Nov 13-16 shows ϵ increases each afternoon (Fig. 2c) over warm SST and enhanced surface
 192 buoyancy flux (Fig 2d). The depth of the mixed layer D also roughly scales with the surface
 193 buoyancy flux $B(0)$ with a sensitivity $dD/d[B(0)] = 460 \text{ m} / 10^{-4} \text{ m}^2 \text{ s}^{-3}$.

194

3. TKE dissipation buoyancy scaling

We scale the amplitude of the dissipation estimates by the surface buoyancy flux B , and average the profiles as a function of the normalized height z/D' , where $D' = 0.95D$. This scaled coordinate centers the composite mixed-layer top on the gradient of the dissipation. The convective (defined by $-D/L > 100$) composite mean profile of scaled dissipation ϵ/B during 2011 Nov 13-16 is shown by black circles in Figure 3.

a. Vertical structure of the convective dissipation profile

The DYNAMO composite scaled dissipation ϵ/B profile is nearly uniform above $z/D' = 0.3$. Close to the surface, for $z/D' \leq 0.25$, the scaled dissipation decreases exponentially from the surface, as $\epsilon/B = E_0 \exp\{-(z/D'H)\}$, with a surface scaled dissipation of $E_0 = 1.45 \pm 0.06$ and a nondimensional scale height of $H = 0.23 \pm 0.01$. The mean dissipation decreases by a factor of about e^{-1} over the observed depth of the surface layer. Mechanical generation of turbulence by shear in this shallow surface layer increases the dissipation relative to the surface buoyancy flux. Mechanical generation and buoyancy flux are correlated because they mutually depend on wind speed. Nondimensional dissipation ϵ/B as a function of $-z/L$ (not shown) is nearly uniform over $-z/L > 50$ and increases in the surface layer, in agreement with aircraft measurements of marine surface layers and the universal function for dissipation (Fairall et al. 1980).

217 Above the surface layer, within $z/D' = [0.4 \ 0.9]$, the mean ϵ/B and its standard error is
 218 0.58 ± 0.02 . The standard deviation of individual ϵ/B estimates is 70-80% of the mean. The
 219 composite dissipation decreases slightly with height, with a linear least-squares fit of
 220 $\epsilon/B = 0.58 - (0.28 \pm 0.05) (z/D' - 0.65)$ (gray lines, Fig. 3b) passing through the mean at
 221 $z/D' = 0.65$.
 222
 223 The scaled dissipation ϵ/B profile for the DYNAMO marine diurnal mixed layer agrees with the
 224 profiles of previously observed convective mixed layers for marine (Lenschow 1970) and
 225 terrestrial (Caughey and Palmer 1979, yellow, Fig. 3) atmospheric boundary layers, subsurface
 226 oceanic convective surface boundary layers (Shay and Gregg 1986: blue and red, Anis and
 227 Moum 1992: green and cyan), and lake convective boundary layers (Imberger 1985, purple).
 228 The vertical mean of the mean and median scaled dissipation ϵ/B for $z/D' = [0.4 \ 0.9]$ is
 229 shown for these studies in Table 1. DYNAMO mean scaled dissipation falls in the middle of the
 230 previous estimates. It is statistically indistinguishable from observations of terrestrial
 231 atmospheric convective mixed layers (Caughey and Palmer 1979) and observations from a Gulf
 232 Stream Ring convective ocean mixed layer (Shay and Gregg 1986).
 233
 234 The composite background dissipation measured above the convective mixed layer is $0.1B$ for
 235 our tropical marine atmosphere, larger than in previous studies (Fig. 3). Moist convection
 236 driven by release of latent heat of condensation in clouds is responsible for intermittent
 237 turbulence above the mixed layer. The distribution of dissipation is positively skewed (skewness

of $\log \epsilon$ is 1-2), indicating infrequent strong events are responsible for much of the turbulence.

The median ϵ/B (0.05) agrees better with previous observations for $z/D' = [1.0 \ 1.4]$.

b. Discussion of the mixed layer dissipation profile

The dissipation in the upper half of the marine convective mixed layer is slightly larger than half the surface buoyancy flux. Dissipation exactly balances buoyancy flux for purely convective turbulence with an equilibrium TKE budget and no mechanical generation or transport of turbulence. Anis and Moum (1994) found a local maximum of dissipation collocated with shear near the top of their convective mixed layers. The maximum near the mixed layer top in the DYNAMO profile is not statistically significant.

Negative buoyancy flux from entrainment of warmer, less dense, air into the mixed layer generates potential energy at the expense of TKE. The TKE is generated locally by shear or transported from the region of positive buoyancy flux below. In stratified geophysical turbulence, negative buoyancy flux is found to be related to dissipation as $B = -\gamma\epsilon$ with $\gamma \approx 0.2$ on average (Winters et al. 1995, Gregg et al. 2018). A typical buoyancy flux for forced entrainment just below the top of the mixed layer is $B(D^-) = -aB(0)$ with $a \approx 0.2$ (Deardorff 1976). The constant a is formally distinct from γ , yet their similar values give $\epsilon(D^-) = a/\gamma B(0) \approx B(0)$. Assuming buoyancy flux linearly decreases with height and dissipation is a piecewise linear function (glancing zero at $z/D' = 5/6$) determined by this scaling, the mean dissipation averaged over $0.5 \leq z/D' < 1$ would be $0.4B(0)$, slightly less than observed.

260

261 Rather than a stable inversion, there is a continuous transition to moist adiabatic stratification
262 at D' . The buoyancy flux at D' is expected to reach zero $\epsilon(D^-) = B(D^-) = 0$ for free
263 entrainment of air with the same density as the mixed layer (Deardorff 1976). Our observed
264 composite mixed layer dissipation at the top of the layer $\epsilon(D^-) = 0.5B(0)$ is midway between
265 this free entrainment condition and the condition of uniform dissipation matching the surface
266 buoyancy flux $\epsilon = B(0)$ throughout the layer.

267

268

269 **4. Connection of diurnal boundary layer convection to clouds**

270

271 The idealized convective dissipation is calculated by multiplying the normalized dissipation
272 profile (Fig. 3) by the time series of surface buoyancy flux $B(0)$. Figure 4a shows this idealized
273 profile of convective dissipation for 2011 Nov 13-16 UTC. Scaled as a function of buoyancy flux,
274 the convective dissipation in the mixed layer increases by a factor of 2.7 in the afternoon
275 compared to at night.

276

277 Mixed layer depth D is also deeper during the afternoon. The height of the mixed layer in Fig.
278 4a is scaled to the observed mixed layer depth D temporally filtered by a 180-min running
279 mean iterated thrice. The Nov 13-16 afternoon maxima of D correspond to maxima in
280 buoyancy flux (Fig. 4b) and convective dissipation (Fig. 4a). When this deeper D reaches the LCL

(also filtered, orange line Fig. 4a), water vapor can condense and form a cloud at the top of the mixed layer.

The mixed layer depth falls below the LCL each evening after sunset. The LCL also lowers gradually at night due to lower temperature and higher relative humidity. The LCL reaches a minimum around dawn (about 0 UTC) when there is weak turbulence and low D . At dawn relative humidity is high as the 10-m dewpoint depression, (green, Fig. 4 b), SST (red), and surface air temperature reach a minimum.

5. Summary

Over vast areas, diurnal convective marine atmospheric mixed layers are dominated by surface buoyancy flux generated over diurnal SST anomalies. A conservative estimate is that $dSST$ reaches at least 1 °C for 5% of days (Prytherch et al. 2013). This fraction of the tropical oceans represents 2% of Earth's surface. The diurnal convective mixed layers are like those over land but with weaker temperature and buoyancy flux anomalies. Weak wind simultaneously makes for weak shear and strong diurnal surface temperature anomalies.

The mean dissipation profile in diurnal convective mixed layers scales with surface buoyancy flux, in agreement with previous observations of convective mixed layers in the atmosphere and ocean (e.g. Lenschow 1970, Caughey and Palmer 1979, Shay and Gregg 1986). The mean

dissipation above the surface layer on 4 days in November 2011 is 0.58 ± 0.02 times the surface buoyancy flux and is nearly constant with height.

Diurnal convective turbulence generates clouds. Mixed layer depth is greater during the afternoon when the DWL and the mixed-layer dissipation is strong. The mixed layer depth reaches the lifting condensation level, where water vapor condenses and forms clouds. The measurements of the diurnal cycle of turbulent kinetic energy dissipation and mixed layer depth are relevant for parameterizing turbulent fluxes into shallow clouds over the parts of the ocean experiencing weak wind, such as during phases of suppressed tropical convective precipitation.

Acknowledgment

The authors gratefully acknowledge J. Moum for conversations and suggestions that motivated this work. The TKE dissipation data is published on the NOAA Chemical Sciences Division web site: <https://esrl.noaa.gov/csl/groups/csl3/measurements/dynamo/calendar.php>. This work was supported by the NOAA OAR Climate Program Office awards NA11OAR4310076 and NA19OAR4310375, Office of Naval Research awards N00014-10-1-0299 and N00014-16-1-3094, and National Science Foundation award 1619903.

Table caption

Table 1. Normalized dissipation over surface buoyancy flux ϵ/B averaged over scaled height $z/D' = [0.4 \ 0.9]$ in convective mixed layers for multiple experiments in lakes, oceans, and the atmosphere. Standard errors of the mean of the variations with height are listed.

Figure captions

Figure 1. (a) Probability distribution of 10-minute SST – predawn SST difference (blue) and daily dSST (red) during 77 days of DYNAMO in Oct 2011 – Jan 2012, (b) relative wind speed, (c) SST, and (d) buoyancy flux.

Figure 2. Time-height series of Doppler lidar dissipation and mixed layer depth D for (a) November 8-December 5, and (c) November 13-16. SST (red), solar radiation (yellow filled), wind speed (black), buoyancy flux (blue) (b,d for times as in a,c). Cloud base height (c, red). Crosses below panels c and d indicate the times of afternoon and nocturnal planview images in supplement S2.

Figure 3. Dissipation ϵ/B scaled by surface buoyancy flux in the marine atmospheric mixed layer (black circles and error bars: mean and standard deviation of the mean; thin black line: median) for DYNAMO convective conditions on Nov 13-16 and for previous estimates for terrestrial atmospheric convective boundary layers (Caughey and Palmer 1979, yellow), subsurface oceanic convective surface boundary layers (Shay and Gregg 1986: blue and red, Anis and Moum 1992: green and cyan), and a lake convective boundary layer (Imberger 1985).

344 (a) Logarithmic scale and (b) linear scale ϵ/B . In (b) gray lines show the best fit relationship
345 $\epsilon/B = 0.58 - (0.28 \pm 0.05) (z/D' - 0.65)$ fitted on $z/D' = [0.4 \ 0.9]$.

346

347 Figure 4. (a) Idealized dissipation for a convective mixed layer, reconstructed from the time
348 series of buoyancy flux, diurnal mixed layer height, and the profile of scaled dissipation ϵ/B
349 (Fig. 3) for 2011 Nov 13-16. Mixed layer depth (white) and lifted condensation level (LCL,
350 orange) of surface air temperature and humidity, filtered thrice with a 180-minute moving
351 window. (b) Solar flux (yellow filled), buoyancy flux (blue), SST (red), and 10-m air dewpoint
352 depression ($T - T_d$, green).

References

- Amaya, D. J., A. J. Miller, S.-P. Xie, and Y. Kosaka, 2020: Physical drivers of the summer 2019 North Pacific marine heatwave. *Nature Communications*, **11**, 1903, <https://doi.org/10.1038/s41467-020-15820-w>.
- Anis, A., & Moum, J. N. (1992). The Superadiabatic Surface Layer of the Ocean during Convection. *Journal of Physical Oceanography*, *22*(10), 1221–1227. [https://doi.org/10.1175/1520-0485\(1992\)022<1221:TSSLOT>2.0.CO;2](https://doi.org/10.1175/1520-0485(1992)022<1221:TSSLOT>2.0.CO;2)
- Anis, A., & Moum, J. N. (1994). Prescriptions for Heat Flux and Entrainment Rates in the Upper Ocean during Convection. *Journal of Physical Oceanography*, *24*(10), 2142–2155. [https://doi.org/10.1175/1520-0485\(1994\)024<2142:PFHFAE>2.0.CO;2](https://doi.org/10.1175/1520-0485(1994)024<2142:PFHFAE>2.0.CO;2)
- Bellenger, H., Takayabu, Y. N., Ushiyama, T., & Yoneyama, K. (2010). Role of Diurnal Warm Layers in the Diurnal Cycle of Convection over the Tropical Indian Ocean during MISO. *Monthly Weather Review*, *138*(6), 2426–2433. <https://doi.org/10.1175/2010MWR3249.1>
- Bellenger, Hugo, & Duvel, J.-P. (2009). An Analysis of Tropical Ocean Diurnal Warm Layers. *Journal of Climate*, *22*(13), 3629–3646. <https://doi.org/10.1175/2008JCLI2598.1>
- Caughey, S. J., & Palmer, S. G. (1979). Some aspects of turbulence structure through the depth of the convective boundary layer. *Quarterly Journal of the Royal Meteorological Society*, *105*(446), 811–827. <https://doi.org/10.1002/qj.49710544606>
- Chen, S. S., & Houze, R. A. (1997). Diurnal variation and life-cycle of deep convective systems over the tropical pacific warm pool. *Quarterly Journal of the Royal Meteorological Society*, *123*(538), 357–388. <https://doi.org/10.1002/qj.49712353806>

374 Clayson, C. A., & Bogdanoff, A. S. (2013). The Effect of Diurnal Sea Surface Temperature
 375 Warming on Climatological Air–Sea Fluxes. <https://doi.org/10.1175/JCLI-D-12-00062.1>

376 Clayson, C. A., & Weitlich, D. (2007). Variability of Tropical Diurnal Sea Surface Temperature.
 377 *Journal of Climate*, 20(2), 334–352. <https://doi.org/10.1175/JCLI3999.1>

378 Dai, A., & Trenberth, K. E. (2004). The Diurnal Cycle and Its Depiction in the Community Climate
 379 System Model. *Journal of Climate*, 17(5), 930–951. [https://doi.org/10.1175/1520-](https://doi.org/10.1175/1520-0442(2004)017<0930:TDCAID>2.0.CO;2)
 380 [0442\(2004\)017<0930:TDCAID>2.0.CO;2](https://doi.org/10.1175/1520-0442(2004)017<0930:TDCAID>2.0.CO;2)

381 Deardorff, J. W. (1976). On the entrainment rate of a stratocumulus-topped mixed layer.
 382 *Quarterly Journal of the Royal Meteorological Society*, 102(433), 563–582.
 383 <https://doi.org/10.1002/qj.49710243306>

384 Fairall, C. W., Markson, R., Schacher, G. E., & Davidson, K. L. (1980). An aircraft study of
 385 turbulence dissipation rate and temperature structure function in the unstable marine
 386 atmospheric boundary layer. *Boundary-Layer Meteorology*, 19(4), 453–469.
 387 <https://doi.org/10.1007/BF00122345>

388 Fairall, C. W., Bradley, E. F., Rogers, D. P., Edson, J. B., & Young, G. S. (1996). Bulk
 389 parameterization of air-sea fluxes for Tropical Ocean-Global Atmosphere Coupled-Ocean
 390 Atmosphere Response Experiment. *Journal of Geophysical Research*, 101(C2), 3747–3764.

391 Frehlich, R., Meillier, Y., Jensen, M. L., Balsley, B., & Sharman, R. (2006). Measurements of
 392 Boundary Layer Profiles in an Urban Environment. *Journal of Applied Meteorology and*
 393 *Climatology*, 45(6), 821–837. <https://doi.org/10.1175/JAM2368.1>

394 Frisch, A. S., & Ochs, G. R. (1975). A Note on the Behavior of the Temperature Structure
 395 Parameter in a Convective Layer Capped by a Marine Inversion. *Journal of Applied*

396 *Meteorology*, 14(3), 415–419. <https://doi.org/10.1175/1520->

397 [0450\(1975\)014<0415:ANOTBO>2.0.CO;2](https://doi.org/10.1175/1520-0450(1975)014<0415:ANOTBO>2.0.CO;2)

398 Gentemann, C. L., & Akella, S. (2018). Evaluation of NASA GEOS-ADAS Modeled Diurnal

399 Warming Through Comparisons to SEVIRI and AMSR2 SST Observations. *Journal of*

400 *Geophysical Research: Oceans*, 123(2), 1364–1375. <https://doi.org/10.1002/2017JC013186>

401 Gentemann, Chelle L., Donlon, C. J., Stuart-Menteth, A., & Wentz, F. J. (2003). Diurnal signals in

402 satellite sea surface temperature measurements. *Geophysical Research Letters*, 30(3),

403 1140. <https://doi.org/10.1029/2002GL016291>

404 Gray, W. M., & Jacobson, R. W. (1977). Diurnal Variation of Deep Cumulus Convection. *Monthly*

405 *Weather Review*, 105(9), 1171–1188. <https://doi.org/10.1175/1520->

406 [0493\(1977\)105<1171:DVODCC>2.0.CO;2](https://doi.org/10.1175/1520-0493(1977)105<1171:DVODCC>2.0.CO;2)

407 Gregg, M. C., D’Asaro, E. A., Riley, J. J., & Kunze, E. (2018). Mixing Efficiency in the Ocean.

408 *Annual Review of Marine Science*, 10(1), 443–473. [https://doi.org/10.1146/annurev-](https://doi.org/10.1146/annurev-marine-121916-063643)

409 [marine-121916-063643](https://doi.org/10.1146/annurev-marine-121916-063643)

410 Grund, C. J., Banta, R. M., George, J. L., Howell, J. N., Post, M. J., Richter, R. A., & Weickmann, A.

411 M. (2001). High-Resolution Doppler Lidar for Boundary Layer and Cloud Research. *Journal*

412 *of Atmospheric and Oceanic Technology*, 18(3), 376–393. <https://doi.org/10.1175/1520->

413 [0426\(2001\)018<0376:HRDLFB>2.0.CO;2](https://doi.org/10.1175/1520-0426(2001)018<0376:HRDLFB>2.0.CO;2)

414 Holbrook, N. J., Scannell, H. A., Sen Gupta, A., Benthuyssen, J. A., Feng, M., Oliver, E. C. J., et al.

415 (2019). A global assessment of marine heatwaves and their drivers. *Nature*

416 *Communications*, 10(1), 2624. <https://doi.org/10.1038/s41467-019-10206-z>

417 Howard, L. (1803). *On the Modification of Clouds*. Retrieved from
 418 https://digital.nmla.metoffice.gov.uk/SO_0f0df589-3560-4ecf-815d-0b9285e6608a/

419 Hughes, K. G., J. N. Moum, and E. L. Shroyer, 2020: Heat Transport through Diurnal Warm
 420 Layers. *J. Phys. Oceanogr.*, **50**, 2885–2905, <https://doi.org/10.1175/JPO-D-20-0079.1>.

421 Imberger, J. (1985). The diurnal mixed layer. *Limnology and Oceanography*, *30*(4), 737–770.
 422 <https://doi.org/10.4319/lo.1985.30.4.0737>

423 Kaimal, J. C. (1973). Turbulence spectra, length scales and structure parameters in the stable
 424 surface layer. *Boundary-Layer Meteorology*, *4*(1), 289–309.
 425 <https://doi.org/10.1007/BF02265239>

426 Kawai, Y., & Wada, A. (2007). Diurnal sea surface temperature variation and its impact on the
 427 atmosphere and ocean: A review. *Journal of Oceanography*, *63*(5), 721–744.
 428 <https://doi.org/10.1007/s10872-007-0063-0>

429 Kolmogorov, A. N. (1941). Dissipation of energy in locally isotropic turbulence (Vol. 32, pp. 16–
 430 18). Presented at the Dokl. Akad. Nauk SSSR.

431 LeMone, M. A., & Pennell, W. T. (1976). The Relationship of Trade Wind Cumulus Distribution to
 432 Subcloud Layer Fluxes and Structure. *Monthly Weather Review*, *104*(5), 524–539.
 433 [https://doi.org/10.1175/1520-0493\(1976\)104<0524:TROTWC>2.0.CO;2](https://doi.org/10.1175/1520-0493(1976)104<0524:TROTWC>2.0.CO;2)

434 Lenschow, D. H. (1970). Airplane Measurements of Planetary Boundary Layer Structure. *Journal*
 435 *of Applied Meteorology*, *9*(6), 874–884. [https://doi.org/10.1175/1520-](https://doi.org/10.1175/1520-0450(1970)009<0874:AMOPBL>2.0.CO;2)
 436 [0450\(1970\)009<0874:AMOPBL>2.0.CO;2](https://doi.org/10.1175/1520-0450(1970)009<0874:AMOPBL>2.0.CO;2)

437 Liu, W. T., Katsaros, K. B., & Businger, J. A. (1979). Bulk Parameterization of Air-Sea Exchanges
 438 of Heat and Water-Vapor Including the Molecular Constraints at the Interface. *Journal of*
 439 *the Atmospheric Sciences*, 36(9), 1722–1735.

440 Madden, R. A., & Julian, P. R. (1971). Detection of a 40-50 day oscillation in the zonal wind in
 441 the tropical Pacific. *Journal of the Atmospheric Sciences*, 28(5), 702–708.

442 Matthews, A. J., Baranowski, D. B., Heywood, K. J., Flatau, P. J., & Schmidtko, S. (2014). The
 443 Surface Diurnal Warm Layer in the Indian Ocean during CINDY/DYNAMO. *Journal of*
 444 *Climate*, 27(24), 9101–9122. <https://doi.org/10.1175/JCLI-D-14-00222.1>

445 Merchant, C. J., M. J. Filippiak, P. L. Borgne, H. Roquet, E. Autret, J.-F. Piollé, and S. Lavender,
 446 2008: Diurnal warm-layer events in the western Mediterranean and European shelf seas.
 447 *Geophysical Research Letters*, 35, <https://doi.org/10.1029/2007GL033071>.

448 Moulin, A. J., Moum, J. N., & Shroyer, E. L. (2017). Evolution of Turbulence in the Diurnal Warm
 449 Layer. *Journal of Physical Oceanography*, 48(2), 383–396. [https://doi.org/10.1175/JPO-D-](https://doi.org/10.1175/JPO-D-17-0170.1)
 450 [17-0170.1](https://doi.org/10.1175/JPO-D-17-0170.1)

451 Moum, J. N., de Szoeke, S. P., Smyth, W. D., Edson, J. B., DeWitt, H. L., Moulin, A. J., et al.
 452 (2014). Air–Sea Interactions from Westerly Wind Bursts During the November 2011 MJO in
 453 the Indian Ocean. *Bulletin of the American Meteorological Society*, 95(8), 1185–1199.
 454 <https://doi.org/10.1175/BAMS-D-12-00225.1>

455 Prytherch, J., Farrar, J. T., & Weller, R. A. (2013). Moored surface buoy observations of the
 456 diurnal warm layer. *Journal of Geophysical Research: Oceans*, 118(9), 4553–4569.
 457 <https://doi.org/10.1002/jgrc.20360>

458 Randall, D. A., Harshvardhan, & Dazlich, D. A. (1991). Diurnal Variability of the Hydrologic Cycle
 459 in a General Circulation Model. *Journal of the Atmospheric Sciences*, 48(1), 40–62.
 460 [https://doi.org/10.1175/1520-0469\(1991\)048<0040:DVOTHC>2.0.CO;2](https://doi.org/10.1175/1520-0469(1991)048<0040:DVOTHC>2.0.CO;2)

461 Ruppert, J. H., & Johnson, R. H. (2016). On the cumulus diurnal cycle over the tropical warm
 462 pool. *Journal of Advances in Modeling Earth Systems*.
 463 <https://doi.org/10.1002/2015MS000610>

464 Ruppert, J. H., Jr., & Johnson, R. H. (2015). Diurnally Modulated Cumulus Moistening in the
 465 Preonset Stage of the Madden–Julian Oscillation during DYNAMO. *Journal of the*
 466 *Atmospheric Sciences*, 72(4), 1622–1647. <https://doi.org/10.1175/JAS-D-14-0218.1>

467 Shay, T. J., & Gregg, M. C. (1986). Convectively Driven Turbulent Mixing in the Upper Ocean.
 468 *Journal of Physical Oceanography*, 16(11), 1777–1798. [https://doi.org/10.1175/1520-](https://doi.org/10.1175/1520-0485(1986)016<1777:CDTMIT>2.0.CO;2)
 469 [0485\(1986\)016<1777:CDTMIT>2.0.CO;2](https://doi.org/10.1175/1520-0485(1986)016<1777:CDTMIT>2.0.CO;2)

470 de Szoeki, S. P., Edson, J. B., Marion, J. R., Fairall, C. W., & Bariteau, L. (2015). The MJO and Air-
 471 Sea Interaction in TOGA COARE and DYNAMO. *Journal of Climate*, 28(2), 597–622.
 472 <https://doi.org/10.1175/JCLI-D-14-00477.1>

473 de Szoeki, S. P., Skillingstad, E. D., Zuidema, P., & Chandra, A. S. (2017). Cold Pools and Their
 474 Influence on the Tropical Marine Boundary Layer. *Journal of the Atmospheric Sciences*,
 475 74(4), 1149–1168. <https://doi.org/10.1175/JAS-D-16-0264.1>

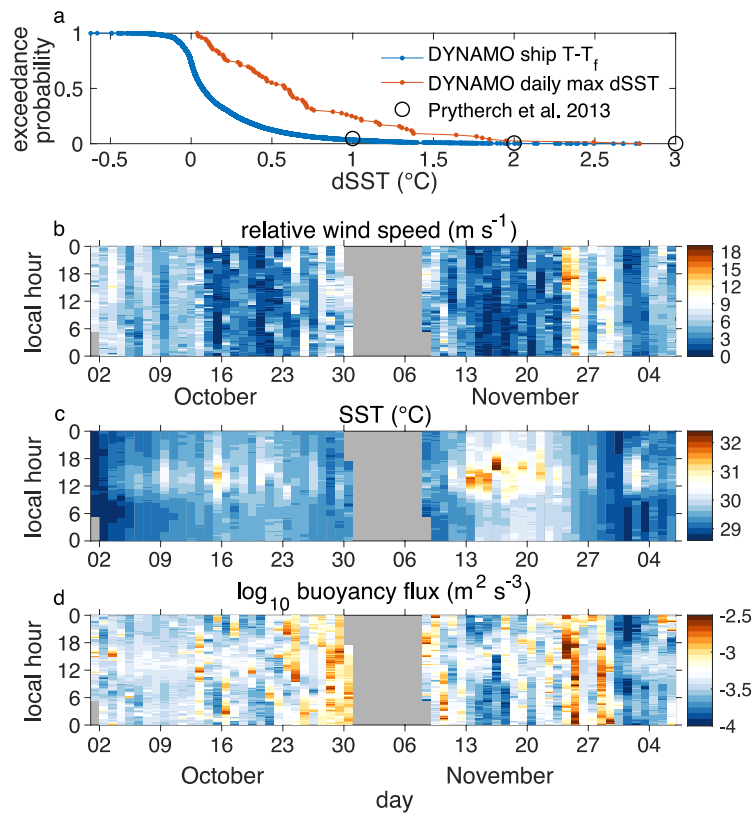
476 Tian, B., Soden, B. J., & Wu, X. (2004). Diurnal cycle of convection, clouds, and water vapor in
 477 the tropical upper troposphere: Satellites versus a general circulation model. *Journal of*
 478 *Geophysical Research: Atmospheres*, 109(D10). <https://doi.org/10.1029/2003JD004117>

479 Winters, K. B., Lombard, P. N., Riley, J. J., & D'Asaro, E. A. (1995). Available potential energy and
480 mixing in density-stratified fluids. *Journal of Fluid Mechanics*, 289, 115–128.
481 <https://doi.org/10.1017/S002211209500125X>

482 Wulfmeyer, V., & Janjić, T. (2005). Twenty-Four-Hour Observations of the Marine Boundary
483 Layer Using Shipborne NOAA High-Resolution Doppler Lidar. *Journal of Applied*
484 *Meteorology*, 44(11), 1723–1744. <https://doi.org/10.1175/JAM2296.1>

485 Yasunaga, K., Fujita, M., Ushiyama, T., Yoneyama, K., Takayabu, Y. N., & Yoshizaki, M. (2008).
486 Diurnal Variations in Precipitable Water Observed by Shipborne GPS over the Tropical
487 Indian Ocean. *Sola*, 4, 97–100. <https://doi.org/10.2151/sola.2008-025>

488 Figures



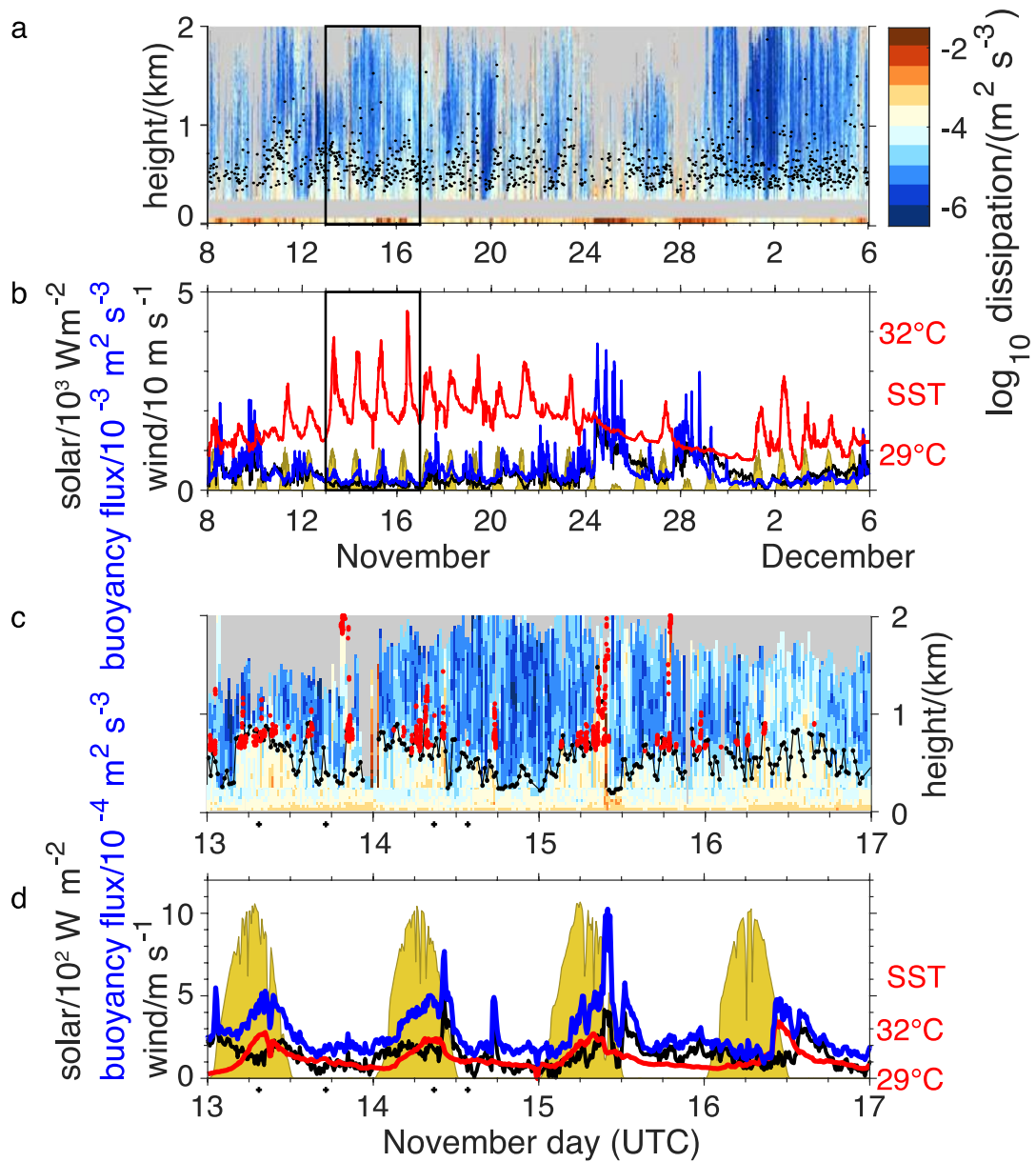
489

490

491 Figure 1. (a) Probability distribution of 10-minute SST – predawn SST difference (blue) and daily

492 dSST (red) during 77 days of DYNAMO in Oct 2011 – Jan 2012, (b) relative wind speed, (c) SST,

493 and (d) buoyancy flux.



495

496 Figure 2. Time-height series of Doppler lidar dissipation and mixed layer depth D for (a)

497 November 8-December 5, and (c) November 13-16. SST (red), solar radiation (yellow filled),

498 wind speed (black), buoyancy flux (blue) (b,d for times as in a,c). Cloud base height (c, red).

499 Crosses below panels c and d indicate the times of afternoon and nocturnal planview images in

500 supplement S2.

weak wind days: 2011 Nov 13-17

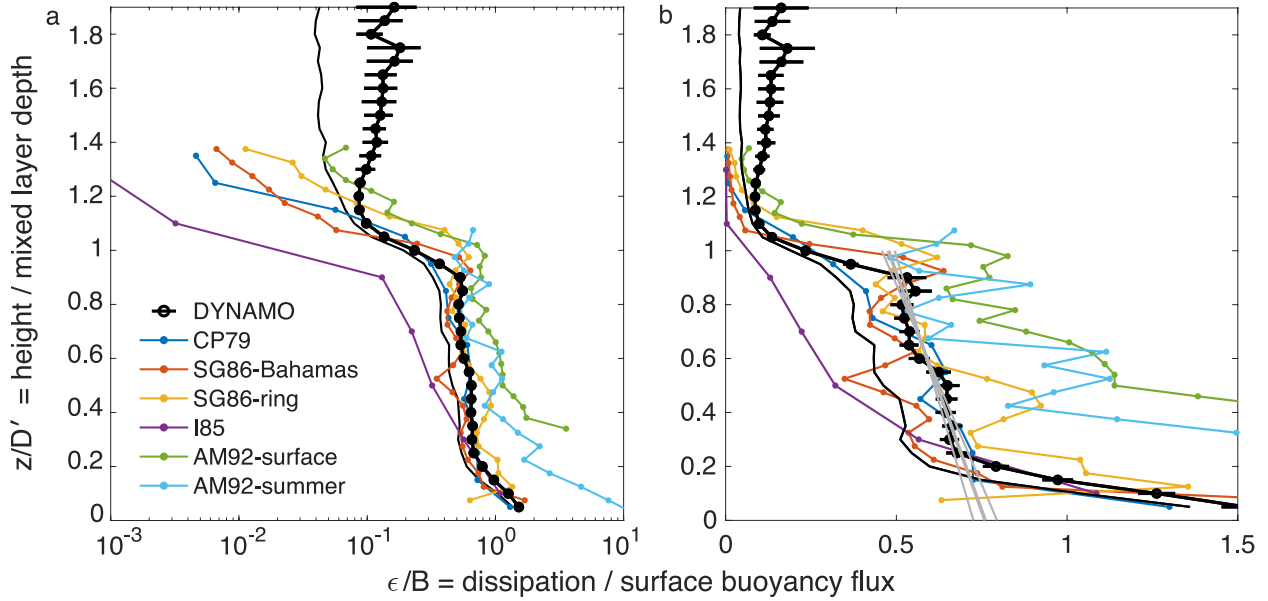


Figure 3. Dissipation ϵ/B scaled by surface buoyancy flux in the marine atmospheric mixed layer (black circles and error bars: mean and standard deviation of the mean; thin black line: median) for DYNAMO convective conditions on Nov 13-16 and for previous estimates for terrestrial atmospheric convective boundary layers (Caughey and Palmer 1979, yellow), subsurface oceanic convective surface boundary layers (Shay and Gregg 1986: blue and red, Anis and Moum 1992: green and cyan), and a lake convective boundary layer (Imberger 1985). (a) Logarithmic scale and (b) linear scale ϵ/B . In (b) gray lines show the best fit relationship $\epsilon/B = 0.58 - (0.28 \pm 0.05) (z/D' - 0.65)$ fitted on $z/D' = [0.4 \ 0.9]$.

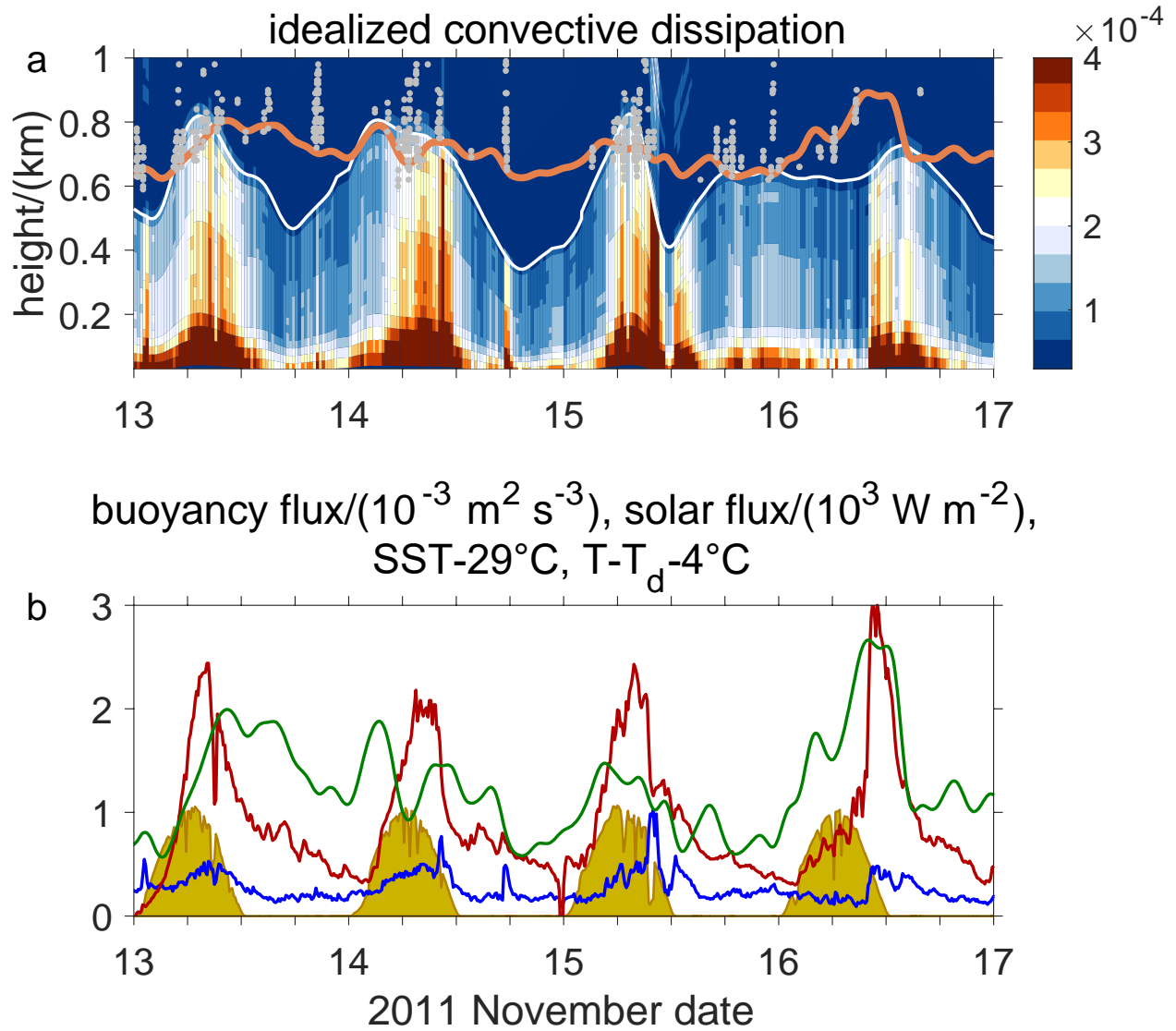


Figure 4. (a) Idealized dissipation for a convective mixed layer, reconstructed from the time series of buoyancy flux, diurnal mixed layer height, and the profile of scaled dissipation ϵ/B (Fig. 3) for 2011 Nov 13-16. Mixed layer depth (white) and lifted condensation level (LCL, orange) of surface air temperature and humidity, filtered thrice with a 180-minute moving window. (b) Solar flux (yellow filled), buoyancy flux (blue), SST (red), and 10-m air dewpoint depression ($T - T_d$, green).

518 Table 1. Normalized dissipation over surface buoyancy flux ϵ/B averaged over scaled height
519 $z/D' = [0.4 \ 0.9]$ in convective mixed layers for multiple experiments in lakes, oceans, and the
520 atmosphere. Standard errors of the mean of the variations with height are listed.

521

reference	description	mean	median
Imberger 1985	lake	0.22 ± 0.06	0.22
Shay and Greg 1986	Bahamas ocean	0.47 ± 0.02	0.46
Caughey and Palmer 1979	terrestrial atmosphere	0.53 ± 0.05	0.57
DYNAMO	marine atmosphere	0.58 ± 0.02	0.56
Shay and Greg 1986	Gulf Stream ring	0.63 ± 0.05	0.58
Anis and Moum 1992	summer ocean	0.83 ± 0.07	0.86
Anis and Moum 1992	surface ocean	1.00 ± 0.08	1.01
grand mean		0.61 ± 0.09	0.61
grand median		0.58	0.57

522